LncRNA-*Snhg3* Aggravates Hepatic Steatosis by Regulating PPARγ via SND1/H3K27me3

Xianghong Xie [1], Mingyue Gao [1], Wei Zhao [1], Chunmei Li [1], Weihong Zhang [2], Jiahui Yang [2], Yinliang Zhang [1], Enhui Chen [3], Yanfang Guo [1], Zeyu Guo [1], Minglong Zhang [3], Ebenezeri Erasto Ngowi [4, 5], Heping Wang [1], Xiaoman Wang [1], Yinghan Zhu [3], Yiting Wang [1], Xiaolu Li [1], Hong Yao [2], Li Yan [3], Fude Fang [1], Meixia Li [6, *], Aijun Qiao [4, 5, *], Xiaojun Liu [1, *]

[1] Department of Biochemistry & Molecular Biology, State Key Laboratory of Common Mechanism Research for Major Diseases, Institute of Basic Medical Sciences Chinese Academy of Medical Sciences & School of Basic Medicine Peking Union Medical College, Beijing 100005, China

[2] Department of Microbiology and Immunology, Shanxi Medical University, Taiyuan 030001, China

[3] Department of Pathophysiology, Institute of Basic Medical Sciences Chinese Academy of Medical Sciences & School of Basic Medicine Peking Union Medical College, Beijing 100005, China

[4] Shanghai Institute of Materia Medica, Chinese Academy of Sciences, 555 Zu Chong Zhi Road, Shanghai, 201203, China

[5] Zhongshan Institute for Drug Discovery, Shanghai Institute of Materia Medica, Chinese Academy of Sciences, Zhongshan, 528400, Guangdong Province, China

[6] State Key Laboratory of Brain and Cognitive Science, Institute of Biophysics, Chinese Academy of Sciences, Beijing 100101, China

*** Corresponding author**

Meixia Li, Email: limeixia@ibp.ac.cn

State Key Laboratory of Brain and Cognitive Science, Institute of Biophysics,

Chinese Academy of Sciences

#15, Datun Road, Chaoyang District, Beijing 100101, China

Aijun Qiao, Email: qiaoaijun@simm.ac.cn

Zhongshan Institute for Drug Discovery, Shanghai Institute of Materia Medica, Chinese Academy of Sciences

Zhongshan, 528400, Guangdong Province, China

& Shanghai Institute of Materia Medica, Chinese Academy of Sciences

555 Zu Chong Zhi Road, Shanghai, 201203, China

Xiaojun Liu, Email: xiaojunliu@ibms.pumc.edu.cn

State Key Laboratory of Common Mechanism Research for Major Diseases, Institute of Basic Medical Sciences Chinese Academy of Medical Sciences & School of Basic Medicine Peking Union Medical College

#5 Dongdansantiao, Beijing 100005, China

Abstract

LncRNAs are involved in modulating the individual risk and the severity of progression in metabolic dysfunction-associated fatty liver disease (MASLD), but their precise roles remain largely unknown. This study aimed to investigate the role of lncRNA *Snhg3* in the development and progression of MASLD, along with the underlying mechanisms. *In vitro* and *in vivo* experiments revealed that *Snhg3* is involved in lipid metabolism and steatosis. The result showed that *Snhg3* was significantly downregulated in the liver of high-fat-induced obesity (DIO) mice. Notably, palmitic acid promoted the expression of *Snhg3* and overexpression of *Snhg3* increased lipid accumulation in primary hepatocytes. Furthermore, knock-in and knock-out models showed significant changes in body and liver weight, heat production, total oxygen consumption, and carbon dioxide production.

Hepatocyte-specific *Snhg3* deficiency alleviated hepatic steatosis in DIO mice, whereas overexpression induced the opposite effect. Mechanistically, *Snhg3* promoted the expression, stability and nuclear localization of SND1 protein via interacting with SND1, thereby inducing K63-linked ubiquitination modification of SND1. Moreover, *Snhg3* decreased the H3K27me3 level and induced SND1-mediated chromatin loose remodeling, thus reducing H3K27me3 enrichment at the *Pparγ* promoter and enhancing *Pparγ* expression. In addition, the administration of PPARγ inhibitor T0070907 improved *Snhg3*-aggravated hepatic steatosis. Our study revealed a new signaling pathway, *Snhg3*/SND1/H3K27me3/PPARγ, responsible for MASLD and indicates that lncRNA-mediated epigenetic modification has a crucial role in the pathology of MASLD.

Introduction

Non-alcohol fatty liver disease (NAFLD) is characterized by excess liver fat in the absence of significant alcohol consumption. It can progress from simple steatosis to nonalcoholic steatohepatitis (NASH) and fibrosis and eventually to chronic progressive diseases such as cirrhosis, end-stage liver failure, and hepatocellular carcinoma (***Loomba, Friedman et al., 2021***). In 2020, an international panel of experts led a consensus-driven process to develop a more appropriate term for the disease utilizing a 2-stage Delphi consensus, that is, “metabolic dysfunction-associated fatty liver disease (MASLD)” related to systemic metabolic dysregulation ***(Gofton, Upendran et al., 2023, Rinella, Lazarus et al., 2023***). The pathogenesis of MASLD has not been entirely elucidated. Multifarious factors such as genetic and epigenetic factors, nutritional factors, insulin resistance, lipotoxicity, microbiome, fibrogenesis and hormones secreted from the adipose tissue, are recognized to be involved in the development and progression of MASLD ***(Buzzetti, Pinzani et al., 2016, Friedman, Neuschwander-Tetri et al., 2018, Lee, Kim et al., 2017, Rada, Gonzalez-Rodriguez et al., 2020, Sakurai, Kubota et al., 2021***). Free fatty acids (FFAs), which are central to the pathogenesis of MASLD, originate from

the periphery, mainly via lipolysis of triglyceride in the adipose tissue, or from increased hepatic *de novo* lipogenesis (DNL). Fatty acids in hepatocytes undergo mitochondrial β-oxidation and re-esterification to form triglyceride (TG), which are then exported into the blood as very low-density lipoproteins or stored in lipid droplets. Hepatic lipotoxicity occurs when the disposal of fatty acids through β-oxidation or the formation of TG is overwhelmed, which leads to endoplasmic reticulum (ER) stress, oxidative stress and inflammasome activation (***Friedman et al., 2018***). Collective literature has indicated that a cluster of differentiation 36/fatty acid translocase (CD36) could increase FFAs uptake in the liver and drive hepatosteatosis onset. Under physiological conditions, CD36 expression in hepatocytes was found to be minimal; however, lipid overload or activation of nuclear receptors including peroxisome proliferator-activated receptor α/γ (PPARα/γ) and liver X receptor (LXR), could significantly increase it (***Rada et al., 2020***).

Epigenetics, an inheritable phenomenon occurring without altering the DNA sequence, can regulate gene expression through different forms, including DNA methylation, histone modifications, chromatin remodeling, transcriptional control, and non-coding RNAs (***Mann, 2014***). Histone modifications, including acetylation, methylation, phosphorylation, ubiquitination, ribosylation, and ubiquitin-like protein modification (SUMO), are important epigenetic determinants of chromatin tightness and accessibility (***Chen & Pikaard, 1997***). Histone methylation is associated with chromatin-specific transcriptional activity states; for example, methylation of lysine 4 of histone H3 (H3K4), H3K36 and H3K79 are linked with a transcriptional activation state, and H3K9, H3K27, and H4K20 with transcriptional repression state ***(Pirola & Sookoian, 2020***). Previous studies have illustrated that epigenetics factors including histone modification play key role in lipid metabolism (***Bayoumi, Gronbaek et al., 2020, Byun, Seok et al., 2020, Jun, Kim et al., 2012***). Furthermore, long non-coding RNAs (lncRNAs) are non-coding RNAs with more than 200 bases in length, can be transcribed by RNA polymerase II, and are comparable to mRNA but lack the crucial open reading framework required for translation (***Ng, Lin et al., 2013, Ulitsky & Bartel, 2013***). LncRNAs are involved in epigenetic regulation of gene expression at

different levels and through different molecular mechanisms such as chromatin remodeling, transcriptional regulation and post-transcriptional processing. Previous studies have indicated that lncRNAs are involved in the pathological progress of MASLD ***(Bayoumi et al., 2020, Sommerauer & Kutter, 2022***). Although histone modification and lncRNAs influence the susceptibility to MASLD, their roles in MASLD remain largely unknown.

Small nucleolar RNA host genes (*Snhgs*), a type of lncRNA, serve as host genes for producing intronic snoRNAs and are mainly related to tumor pathophysiology by regulating proliferation, apoptosis, invasion, and migration ***(Sen, Fallmann et al., 2020, Zimta, Tigu et al., 2020***). Here, we found that the expression of hepatic *Snhg3* was decreased in high-fat-induced obesity (DIO) mice. Experiments conducted using *in vivo* and *in vitro* models indicated that *Snhg3* was involved in lipid metabolism and hepatic steatosis. Mechanistically, *Snhg3* interacted with staphylococcal nuclease and Tudor domain containing 1 (SND1), a well-understood Tudor protein that participates in lipid metabolism and tumoral behavior by modulating cholesterol and glycerophospholipid metabolism and acylglyceride storage in lipid droplets ***(Navarro-Imaz, Ochoa et al., 2020***). Furthermore, *Snhg3* increased the expression of SND1 by promoting the stability of SND1 mediated by K63-linked ubiquitination and induced nuclear localization of SND1 protein, thereby reducing tri-methylation at H3K27 (H3K27me3) enrichment and boosting chromatin loose remodeling at PPARγ promoter, eventually enhancing *Pparγ* and *Cd36* expressions.

Results

LncRNA-*Snhg3* is downregulated in high-fat diet-induced obesity mice

Firstly, we analyzed the lncRNAs expression profiles in the livers of DIO mice and normal chow-fed mice (control) by RNA-Seq, and found 18072 hepatic lncRNAs, including 338 differentially expressed lncRNAs (q-value ≤ 0.05, ***Figure 1A -Supplementary Table S1***). Of all *Snhgs*, *Snhg3* had the most prominent expression and exhibited more noticeable downregulation in the liver of the DIO compared to the

control mice (***Figure 1B***); thus, it was selected for further study. The downregulation of *Snhg3* was confirmed by RT-qPCR (***Figure 1C***). Additionally, the Coding Potential Calculator indicated that *Snhg3* has a coding probability of 0.020757, classifying it as a noncoding sequence (***Kang, Yang et al., 2017***). Localization of *Snhg3* was primarily observed in nuclei with a probability score of 0.451138, as predicted using software prediction (http://lin-group.cn/server/iLoc-LncRNA/predictor.php). The exact nuclear localization of *Snhg3* was further confirmed by nuclear/cytoplasmic fractionation (***Figure 1D***).

Hepatocyte-specific *Snhg3* knock-out alleviates hepatic steatosis in DIO mice

Since *Snhg3* was associated with hepatic nutrition change, the role of *Snhg3* was further confirmed by constructing hepatocyte-specific *Snhg3* knock-out (*Snhg3*-HKO) mice (***Figure 2A***). The result indicated that body weight was mildly decreased in DIO *Snhg3*-HKO mice compared with the control DIO *Snhg3*-Flox mice (***Figure 2B***). The energy consumption is mainly reflected as the sum of energy utilization during internal heat production using comprehensive laboratory animal monitoring system (CLAMS). DIO *Snhg3*-HKO mice had higher heat production, total oxygen consumption, and carbon dioxide production (***Figure 2C and D***). Conversely, the respiratory exchange ratio (RER) showed no difference (***Figure 2E***). Furthermore, insulin sensitivity, not glucose tolerance, was improved in DIO *Snhg3*-HKO mice (***Figure 2F***). The DIO *Snhg3*-HKO mice had a decrease in liver weight and the ratio of liver weight/body weight, and improved hepatic steatosis, including decreasing lipid accumulations and the ballooning degeneration of liver cells (***Figure 2G-I***). Serum alanine transaminase (ALT) and aspartate transaminase (AST) levels were significantly decreased in *Snhg3*-HKO mice (***Figure 2J***). In addition, serum FFAs, TG and TC were also reduced in *Snhg3*-HKO mice (***Figure 2K***). The DIO *Snhg3*-HKO mice exhibited a decrease in inguinal white adipose tissue (iWAT) weight and the ratio of iWAT weight/body weight, but not in brown adipose (BAT) weight and the ratio of BAT weight/body weight (***Figure 2L***). And there was no

difference in serum insulin between DIO *Snhg3*-HKO mice and control mice (***Figure 2M***). These results suggested that hepatic knockout of *Snhg3* improves hepatic steatosis in DIO mice.

Hepatocyte-specific *Snhg3* knock-in aggravates hepatic steatosis in DIO mice

Furthermore, the hepatocyte-specific *Snhg3* knock-in (*Snhg3*-HKI) mice were also constructed to detect the function of *Snhg3* in the liver (***Figure 3A***). The DIO *Snhg3*-HKI mice showed greater weight gains than the control wild type (WT) mice (***Figure 3B***). In addition, DIO *Snhg*3-HKI mice had lower heat production, total oxygen consumption, and carbon dioxide production (***Figure 3C and D***). The RER result indicated the DIO *Snhg3*-HKI mice utilized less fat (***Figure 3E***). Insulin sensitivity was also impaired in DIO *Snhg3*-HKI mice (***Figure 3F***). The liver weight and the ratio of liver weight/body weight of DIO *Snhg3*-HKI mice were markedly increased (***Figure 3G***). Also, DIO *Snhg3*-HKI mice exhibited severe hepatic steatosis (***Figure 3H and I***) and higher serum ALT and AST levels (***Figure 3J***). Both serum TC and iWAT weight were increased in DIO *Snhg3*-HKI mice (***Figure 3K and L***). Similar to DIO *Snhg3*-HKO mice, there was also no difference in serum insulin between DIO *Snhg3*-HKI mice and WT mice (***Figure 3M***). These findings indicated that upregulation of *Snhg*3 could promote DIO hepatic steatosis.

***Snhg3* promotes hepatic steatosis by regulating chromatin remodeling**

To clarify the molecular mechanism of *Snhg3* in hepatic steatosis, we investigated the hepatic differentially expressed genes (DEGs) using RNA-Seq. There were 1393 DEGs between the DIO *Snhg3*-HKI and control WT mice, with 1028 genes being upregulated and 365 genes downregulated (log2FC $\geq$ 1, q-value $<$ 0.001) in the liver of *Snhg3*-HKI mice (***Figure 4A - Supplementary Table S2***). A gene set enrichment analysis (GSEA) of DEGs revealed that *Snhg3* exerts a global effect on the expression of genes involved in fatty acid metabolism and the PPAR signaling pathway (***Figure 4B***).

LncRNAs in the nucleus can affect gene expression in multiple ways, such as chromatin remodeling, transcriptional regulation, and post-transcriptional processing (***Morey & Avner, 2004, Thomson & Dinger, 2016***). Since *Snhg3* was mainly localized in the nuclei of hepatocytes, we next checked the genome-wide chromatin accessibility (log2FC > 2, p-value < 0.001) in the liver of DIO *Snhg3*-HKI and WT mice using ATAC-Seq. We discovered that in all 6810 differentially accessible regions (DARs), 4305 (> 63.2%) were more accessible in *Snhg3*-HKI mice and only 2505 (> 36.8%) of peaks were more accessible in control mice (Supplementary Table S3), indicating that the chromatin states were 'hyper-accessible' in the liver of *Snhg3*-HKI mice. Moreover, DARs were with relatively few promoter-proximal (Up2k) and exon regions in both the control and *Snhg3*-HKI groups (***Figure 4C***), supporting the idea that gene activation depends on multiple regulatory regions, is not limited to its promoter and exon regions (***Ackermann, Wang et al., 2016***). Furthermore, 3966 genes were associated specifically with the accessible regions in the *Snhg3*-HKI group and only 2451 genes in the WT group (log2FC > 2, p-value < 0.001, ***Supplementary Table S4***). Additionally, *PPARγ* was identified as a potential transcription factor associated with hyper-accessible regions in the liver of the *Snhg3*-HKI group by HOMER and CREMA (***Figure 4D and E***).

To determine whether open chromatin regions were correlated with gene expression, we integrated ATAC-Seq data (genes associated with DARs, log2FC > 2, p-value < 0.001) with RNA-Seq data (DEGs in DIO *Snhg3*-HKI and control mice, log2FC > 1, q-value < 0.001). Overall, 233 upregulated genes shown in quadrant 2, including *Cd36* and cell death-inducing DNA fragmentation factor 45 like effector a/c (*Cidea/c*), which are critical for MASLD progression (***Koonen, Jacobs et al., 2007, Matsusue, Kusakabe et al., 2008, Sans, Bonnafous et al., 2019***), had at least one associated open chromatin region, which accounted for >22.67% (total 1028) of DEGs mapped to ATAC-Seq peaks in the liver of *Snhg3*-HKI mice (***Figure 4F-H - Supplementary Table S5***). Meanwhile, at least one open chromatin region was associated with 65 downregulated genes in the quadrant 3, which accounted for > 17.81% (total 365) of DEGs mapped to ATAC-Seq peaks in the liver of WT mice

(***Figure 4F - Supplementary Table S5***). Furthermore, the expression levels of *Cd36* and *Cidea* in the liver of *Snhg3*-HKO and *Snhg3*-HKI mice were confirmed by RT-qPCR and western blotting (***Figure 4I and J***).

Snhg3 induces SND1 expression by interacting with SND1 and enhancing the stability of SND1 protein

To further elucidate the molecular mechanism of *Snhg3* in hepatic steatosis, an RNA pull-down followed by mass spectrometry (MS) assay was performed in primary hepatocytes. The result identified 234 specific *Snhg3*-associated proteins, involved in multiple signaling pathways, including PPAR, NAFLD and fatty acid degradation pathways (***Figure 5A and B - Supplementary Table S6***). Of these proteins, a well-understood Tudor protein SND1 was also predicted to interact with three fragments of *Snhg3* by bioinformatic method (RBPsuite (sjtu.edu.cn)) (***Figure 5C and D - Supplementary Table S7***). *Snhg3* coprecipitation with SND1 was confirmed by RNA pull-down coupled with western blotting (***Figure 5E***), which was consistent with the RNA immunoprecipitation (RIP) assay results (***Figure 5F***). Meanwhile, *Snhg3* regulated the protein, not mRNA, expression of SND1 *in vivo* and *in vitro* by promoting the stability of SND1 protein (***Figure 5G-I***). Furthermore, we tested the effect of *Snhg3* on the ubiquitin-modification of SND1 and found that *Snhg3* enhanced SND1 ubiquitination *in vivo* and *in vitro* (***Figure 5K and L***). Previous studies indicated that K48-linked polyubiquitination aids in proteasome-mediated recognition and degradation and that K63-linked polyubiquitination participates in signaling assemblies and protein stability (***Sun, Liu et al., 2020***). As predicted, *Snhg3* overexpression increased K63-linked ubiquitination modification in endogenous and exogenous SND1 protein, not K48- or K33-linked (***Figure 5M and N***). Additionally, *Snhg3* overexpression enhanced the nuclear localization of SND1 in Hepa1-6 cells with PA treatment (***Figure 5O***). Collectively, these results suggested that *Snhg3* promoted the K63-linked ubiquitination and stability of SND1 protein through interacting with SND1, thus resulting in SND1 protein increase and nuclear localization.

Snhg3 **promotes PPARγ expression by decreasing H3K27me3 enrichment at the** ***Pparγ*** **promoter**

SND1, initially named as p100, is a highly conserved and ubiquitously expressed multifunctional Tudor domain-containing protein that participates in pivotal biological processes like double-stranded RNA editing, pre-mRNA splicing, microRNA-mediating gene silencing and piRNA biogenesis in germlines (***Ying & Chen, 2012***). Previous studies indicated that Tudor proteins participate in epigenetic regulation by binding to methyl-arginine/lysine residues (***Ying & Chen, 2012***). However, whether SND1 influences histone modification remains unclear. It is well known that histone modification dynamically regulates specific gene expression by altering the organization and function of chromatin and is involved in the pathophysiology of some diseases, such as histone H3 methylation modification, which may contribute to MASLD pathogenesis (***Byun et al., 2020, Jun et al., 2012, Tessarz & Kouzarides, 2014***). Considering that H3K27me3, a repressive chromatin mark, plays a role in autophagy-mediated lipid degradation (***Byun et al., 2020***), we tested the effect of SND1 on H3K27me3. The results revealed that both SND1 and *Snhg3* overexpression reduced the H3K27me3 level (***Figure 6A***). Furthermore, disrupting SND1 expression increased the H3K27me3 level and reversed the *Snhg3*-induced H3K27me3 decrease (***Figure 6B and C***). Moreover, the hepatic H3K27me3 level was upregulated in *Snhg3*-HKO mice but downregulated in *Snhg3*-HKI mice (***Figure 6D***). The results indicated that *Snhg3* negatively regulated the H3K27me3 level through SND1.

To further clarify whether *Snhg3*-induced H3K27me3 decrease is involved in hepatic steatosis, we examined the H3K27me3 enrichment in the liver of DIO *Snhg3*-HKO mice using the CUT&Tag assay and detected 10915 peaks (***Supplementary Table S8***). The genomic locations of these peaks were divided into eight categories, and the H3K27me3 signals were predominantly (about 54%) enriched at the 2-kb promoter, 5’-untranslated region (5’-UTR), and exon categories. Meanwhile, very few signals (about 14%) were enriched in the 2-kb downstream and

intergenic categories in the liver of DIO *Snhg3*-HKO mice (***Figure 6E***). Moreover, the exon, upstream2k, 5'-UTR and intron regions of *Pparγ* were enriched with the H3K27me3 mark (fold_enrichment = 4.15697) in the liver of DIO *Snhg3*-HKO mice (***Supplementary Table S8***). Subsequently, ChIP assay revealed that hepatic H3K27me3 enrichment at the *Pparγ* promoter was increased in DIO *Snhg3*-HKO mice but decreased in DIO *Snhg3*-HKI mice (***Figure 6F***). *Snhg3*-overexpression in Hepa1-6 cells yielded similar results (***Figure 6G***).

SND1 mediates *Snhg3*-induced PPARγ expression increase

Collective studies have indicated that PPARγ plays a crucial role in MASLD progression by regulating target genes such as *Cd36* and *Cidec* ***(Lee, Muratalla et al., 2023b, Lee, Pusec et al., 2021, Lee, Park et al., 2018, Matsusue et al., 2008, Skat-Rordam, Hojland Ipsen et al., 2019***). In this study, the mRNA and protein expression levels of hepatic PPARγ were decreased in DIO *Snhg3*-HKO mice and increased in DIO *Snhg3*-HKI mice (***Figure 7A and B***). The upregulation of *Snhg3* and SND1 also increased the expression of *Pparγ* and *Cd36 in vitro* (***Figure 7C-E***). Meanwhile, disruption of SND1 expression alleviated *Snhg3*-induced PPARγ and CD36 increase and lipid accumulation (***Figure 7F-H***). Collectively, these results demonstrated that SND1 mediates *Snhg3*-induced PPARγ and CD36 expression.

PPARγ mediates *Snhg3*-induced hepatic steatosis

Hepatocyte-specific depletion of PPARγ is known to protect mice against NASH and boost the therapeutic efficacy of rosiglitazone, a synthetic PPARγ agonist, in the liver (***Lee et al., 2021***). Furthermore, PPARγ is an inducer of adipocyte differentiation and a reservoir for excess FFAs, thereby potentially preventing lipotoxicity in other tissues and organs (***Medina-Gomez, Gray et al., 2007***). To this end, we tested the effect of T0070907, a selective PPARγ inhibitor, on *Snhg3*-induced hepatic steatosis in DIO mice. The result showed that T0070907 treatment for 8 weeks had no effects on body weight, liver and iWAT weight, and serum FFAs, TG and TC in DIO *Snhg3*-HKI mice, but improved *Snhg3*-induced hepatic steatosis in DIO *Snhg3*-HKI

mice (***Figure 8A-E***). Additionally, T0070907 also mitigated the hepatic *Cd36* increase in DIO *Snhg3*-HKI mice and *Snhg3*- and SND1-induced *Cd36* increase in hepa 1-6 cells (***Figure 8F and G***). Collectively, these results suggested that PPARγ-mediated *Snhg3*-induced hepatic steatosis and CD36 increase.

Discussion

Liver steatosis is common in various metabolic diseases and related disorders, including MASLD. Although lncRNAs are implicated in regulating numerous mechanisms related to liver steatosis and MASLD, their exact function remains to be determined. In this study, hepatocyte-specific lncRNA-*Snhg3* deficiency improved hepatic steatosis and insulin resistance, while overexpression aggravated hepatic steatosis and insulin resistance in DIO mice. Excessive hepatic lipid deposition owing to increased FFAs uptake and hepatic DNL impairs autophagy and promotes endoplasmic reticulum stress and oxidative stress, insulin resistance, liver tissue damage, and inflammation, ultimately aggravating MASLD progression (***Rada et al., 2020***). Further evidence suggests that CD36 plays an important role in facilitating intracellular FFAs uptake. Overexpression of CD36 in hepatocytes increased FFAs uptake and TG storage; conversely, its deletion ameliorated hepatic steatosis and insulin resistance in DIO mice (***Rada et al., 2020***). Therefore, CD36 could be a potential biomarker for MASLD diagnosis. As a transcription regulator of CD36, PPARγ plays major adipogenic and lipogenic roles in adipose tissue. Although PPARγ is most abundantly expressed in adipocytes and plays major adipogenic and lipogenic roles in the tissue, it has been reported to also be expressed in hepatocytes. There is a strong correlation between the onset of MASLD and hepatocyte-specific PPARγ expression. Clinical trials have indicated that increased insulin resistance and hepatic PPARγ expressions were associated with NASH scores in some obese patients ***(Lee, Muratalla et al., 2023a, Mukherjee, Wanjari et al., 2022***). Activation of PPARγ in the liver induces the adipogenic program to store fatty acids in lipid droplets as observed in adipocytes ***(Lee et al., 2018***). Moreover, the inactivation of

liver PPARγ abolished rosiglitazone-induced an increase in hepatic TG and improved hepatic steatosis in lipoatrophic AZIP mice (***Gavrilova, Haluzik et al., 2003***). In this study, *Snhg3* overexpression induced an increase in hepatic PPARγ and CD36. Although the administration of PPARγ antagonist T0070907 aggravated hepatic steatosis owing to an inhibition of adipogenesis in adipose tissue, it improved *Snhg3*-induced hepatic steatosis. Even though PPARγ's primary function is in adipose tissue, patients with MASLD have much higher hepatic expression levels of PPARγ, reflecting the fact that PPARγ plays different roles in different tissues and cell types (***Mukherjee et al., 2022***). Thus, understanding how the hepatic PPARγ expression is regulated will help develop prevention and treatments for MASLD (***Lee et al., 2018***).

Epigenetics plays a crucial role in many physiological and pathological situations (***Peixoto, Cartron et al., 2020***). Epigenetic regulation induces phenotypic changes that may respond to environmental cues through DNA methylation and histone modification, chromatin remodeling, and noncoding RNAs (***Mann, 2014***). Epigenetic changes interact with inherited risk factors to modulate the individual risk of MASLD development and the severity of progression. Epigenetic modifications, including DNA methylation, miRNAs, and histone modifications, have been associated with MASLD (***Baffy, 2015, Eslam, Valenti et al., 2018, Jonas & Schurmann, 2021***). To date, there is no approved pharmacologic therapy for MASLD, and the mainstay of management remains lifestyle changes with exercise and dietary modifications ***(Bayoumi et al., 2020***). Therefore, understanding the epigenetic modifications in MASLD pathogenesis might prove a rational strategy to prevent the disease and develop novel therapeutic interventions (***Sodum, Kumar et al., 2021***).

LncRNAs, being abundant in the genome participate in regulating the expression of coding genes through various molecular mechanisms, including: (1) transcriptional regulation at the promoter of target genes; (2) inhibiting RNA polymerase II or mediating chromatin remodeling and histone modification; (3) interfering with the splicing and processing of mRNA or producing endogenous siRNA; (4) regulating the activity or cellular localization of the target protein; (5) acting as competitive endogenous RNAs; and (6) riboregulation by forming nucleic acid-protein complex as

structural component ***(Morey & Avner, 2004, Sommerauer & Kutter, 2022, Thomson & Dinger, 2016***). However, compared to the large number of lncRNAs, only few have been functionally well-characterized. Collective literature has shown that lncRNAs play a crucial role in MASLD (***Sommerauer & Kutter, 2022***). This study demonstrated that lncRNA-*Snhg3* participated in the pathology of MASLD by epigenetic modification; that is, *Snhg3* inhibited the H3K27me3 level, and promoted chromatin relaxation at the *Pparγ* promoter and eventually increased PPARγ expression. The results from Ruan et al. demonstrated that more than a third of dynamically expressed lncRNAs were deregulated in a human MASLD cohort and the lncRNA human lncRNA metabolic regulator 1 (hLMR1) positively regulated transcription of genes involved in cholesterol metabolism (***Ruan, Li et al., 2021***). Previous studies have also demonstrated that several lncRNAs, including FLRL2/3/6/7/8, H19, and MALAT-1, were associated with lipogenesis via proteins in the PPAR signaling pathway (***Mukherjee et al., 2022***). Recently, a murine long noncoding single-cell transcriptome analysis elucidated liver lncRNA cell-type specificities, spatial zonation patterns, associated regulatory networks, and temporal patterns of dysregulation during hepatic disease progression. Moreover, a subset of the liver disease-associated regulatory lncRNAs identified have human orthologs (***Karri & Waxman, 2023***). Based on the aforementioned information, lncRNAs emerge as promising candidates for biomarkers and therapeutic targets for MASLD.

Tudor proteins play vital roles in normal cell viability and growth by diverse epigenetic functions, including methylation dependent chromatin-remodeling, histone-binding, pre-RNA-processing, RNA-silencing, and transposon silencing in ligands (***Ying & Chen, 2012***). Tudor proteins are divided into four groups: Group1 Tudor proteins bind to methyl-lysine⁄arginine of histone tails, including Tdrd3, PHF1, PHF20, the JMJD family and TP53BP1; Group 2 Tudor proteins bind to methyl-arginine of ligands and representative members include SMN and SMNDC1; Group 3 is represented by SND1; and Group 4, contains many Tudor proteins, including Tdrd1-9 and Tdrd11, that have been identified in methylation-dependent association with PIWI proteins Ago3, Aub and Piwi. Some studies suggested that

SND1 plays important roles in cancer by interacting with other transcription factors, including PPARγ, signal transducer and activator of transcription 5/6 (STAT6/5) and myeloblastosis oncogene (c-Myb) (***Duan, Zhao et al., 2014, Navarro-Imaz et al., 2020***). SND1 could induce adipogenesis and promote the formation of lipid droplets in adipocytes through working as a co-activator of PPARγ and regulating H3 acetylation (***Duan et al., 2014***). Our study showed that both *Snhg3* and SND1 decreased the H3K27me3 level and promoted the expression of PPARγ. SND1 could interact with *Snhg3* and mediate the *Snhg3*-induced decrease in H3K27me3 and increase in *Pparγ* and *Cd36* expressions. Furthermore, inhibition of PPARγ with T0070907 alleviated *Snhg3*- and SND1-induced *Cd36* increase and improved *Snhg3*-aggravated hepatic steatosis. In lncRNA riboregulation, the actions of noncoding RNAs mostly rely on interactions with proteins, including canonical or noncanonical RNA-binding proteins (RBPs). Canonical RBPs, such as heterogeneous nuclear ribonucleoproteins (hnRNPs), polypyrimidine tract binding protein 1 (PTBP1) and human antigen R (HUR), are often involved in posttranscriptional regulation, including pre-mRNA processing, RNA stability, RNA decay, or nuclear export (***Briata & Gherzi, 2020***). Previous studies have demonstrated that some lncRNAs, e.g., LINC01018, MEG3, APOA4-AS, hLMR1, Blnc1 and LncARSR interact with canonical RBPs to govern the progression of MASLD (***Sommerauer & Kutter, 2022***).

In summary, our study demonstrates that lncRNA-*Snhg3* increased the expression, stability, and nuclear localization of SND1 protein by interacting with SND1, thus enhancing the expression of PPARγ via reducing H3K27me3 enrichment and boosting chromatin loose remodeling at the *Pparγ* promoter, ultimately resulting in hepatic steatosis under DIO status (***Figure 8H***). This study reveals a new signaling pathway, *Snhg3*/SND1/H3K27me3/PPARγ, responsible for hepatic steatosis and provides evidence of lncRNA-mediated epigenetics in the pathophysiology of MASLD.

Materials and Methods

Animals and treatments

C57BL/6 *Snhg3*-Flox mice and hepatocyte-specific *Snhg3* knock-in (*Snhg3*-HKI) mice were created using the CRISPR-Cas9 system at Cyagen Biosciences. To engineer the targeting vector for *Snhg3*-Flox mice, the exon 3 of *Snhg3* was selected as the conditional knockout region, and homology arms and the cKO region were generated by PCR using BAC clone as a template. Cas9 and gRNA were co-injected into fertilized eggs with a targeting vector for mice production. The obtained mice were identified by PCR followed by sequence analysis. Hepatocyte-specific *Snhg3* knock-out (*Snhg3*-HKO) mice were generated by crossing *Snhg3*-Flox mice with C57BL/6-Alb-Cre mice. For *Snhg3*-HKI mice, the "Alb promoter-mouse Snhg3 cDNA-polyA" cassette was inserted into an H11 locus (~0.7 kb 5' of the Eif4enif1 gene and ~4.5 kb 3' of the Drg1 gene), and homology arms were generated by PCR using BAC clone as template to engineer the targeting vector. Cas9 and gRNA were co-injected into fertilized eggs with targeting vector for mice production. The obtained mice were identified by PCR followed by sequence analysis. All mice were housed in the pathogen-free conditions (SPF) facility and maintained on a 12 h light-dark cycle and a regular unrestricted diet. All mice were fed either a normal chow diet (9% fat; Lab Diet) or HFD (60% fat, Research Diets) for inducing obesity and libitum with free access to water. Unless otherwise noted, 6~8-week-old male mice were used for all experiments. 8-week-old mice fed on HFD were injected intraperitoneally (i.p.) with 1mg/kg of T0070907 dissolved in DMSO for 5 days per week for 2 months. Liver tissue samples were analyzed by the High Fatty Sample Total Cholesterol (TC) Content Assay Kit (APPLYGEN, Cat#E1025-105) and the High Fatty Sample Triglyceride (TG) Content Assay Kit (APPLYGEN, Cat#E1026-105), respectively. Serum concentrations of ALT, AST, FFAs, TG and TC were determined using an automated Monarch device (Peking Union Medical College Hospital, Beijing, China). Serum insulin was detected using a mouse insulin ELISA kit (JM-02862M1, Beijing BioDee Biotechnology Co., Ltd.). All animal experiments were conducted under protocols approved by the Animal Research Committee of the Institute of Laboratory Animals, Institute of Basic Medical Sciences

Chinese Academy of Medical Sciences & School of Basic Medicine Peking Union Medical College (ACUC-A01-2022-010).

Cell culture

Primary mouse hepatocytes were isolated from 8-week-old male C57BL/6J mice and cultured in RPMI 1640 medium with 10% FBS as previously described ***(Matsumoto, Ogawa et al., 2002***). Hepa 1-6 cells (ATCC, Cat#CRL-1830) were cultured at 37 °C, 5% CO_2 in DMEM (Gibco, Carlsbad, USA) supplemented with 10% FBS, and 1% penicillin-streptomycin. After attachment, the cells were transfected with indicated plasmids or *siSnd1* by Lipofectamine 3000 Transfection Kit (Invitrogen). Cells were treated with and without 0.25 μm PA for 12h - 24h before collection. The sequences of *siSnd1* were #1, TGGAGAACATGCGCAATGACATC; #2, GTGCATGTCTTCTACATCGACTA; #3, GTATTGCCAGCTCAAGCCACAGAGTAT. UUCUCCGAACGUGUCACGUTT was used as a control.

Plasmid construction

Snhg3 was amplified from liver cDNA and was then constructed into pcDNA3.1 and pAd-Track-CMV using Kpn I/EcoR I and Kpn I/EcoR V, respectively. The primers for pcDNA3.1-*Snhg3* were ATATCGGGTACCGACTTCCGGGCGTTAC and ATGATCGAATTCAGACATTCAAATGCT; for pAd-Track-CMV-*Snhg3* were ATATCGGGTACCGACTTCCGGGCGTTAC and ATGATTGATATCAGACATTCAAATGCT.

Real-Time Quantitative PCR (RT-qPCR)

Total RNA was extracted from mouse tissues using a Trizol-based method. Approximately 2 μg of total RNA was reverse-transcribed into a first-strand cDNA pool using reverse transcriptase and random primers, according to the manufacturer's instructions. RT-qPCR was performed using SYBR Green PCR Master Mix (A6002, Promega) with the gene-specific primers (Table S9). All gene expression data were normalized to actin expression levels.

Western blotting

Protein was extracted from frozen tissue samples in cell lysis buffer. In total, protein was loaded onto a 10% SDS-polyacrylamide gel, and separated proteins were transferred to PVDF membranes. Western blot assays were performed using indicated specific antibodies (Table S10). The proteins were quantified by ImageJ software.

Coding potential prediction

The coding potential of *Snhg3* was evaluated by the Coding Potential Calculator at CPC2@CBI,PKU(gao-lab.org) (***Kang et al., 2017***).

Histopathologic analysis

Liver tissue sections were fixed in 4% paraformaldehyde, then embedded in paraffin and stained with H&E to visualize the general morphological and structural characteristics of tissues. Lipid droplet accumulation in the liver was visualized using Oil red O staining of frozen liver sections that were prepared in optimum cutting temperature (O.C.T.) compound.

Subcellular fractionation

A Cytoplasmic & Nuclear fraction Kit (Beyotime Biotechnology, China) was used to detect *Snhg3* expression in cytoplasmic and nuclear fractions. RNA was extracted from the cytoplasmic and nuclear fractions using a Trizol-based method and subjected to qPCR. *Gapdh* was used as a cytoplasmic marker, and *Neat1* and *Xist* were used as a nuclear marker. The percentage of the transcript abundance was calculated using the following formula, Nucleus % = $2^{\wedge Ct(Nucleus)}/(2^{\wedge Ct(Cytoplasm)} + 2^{\wedge Ct(Nucleus)})$, Cytoplasm % = 1- Nucleus %.

Mouse Calorimetry

Male mice were housed individually in metabolic chambers of an Oxymax system (Columbus Instruments). The first readings were taken after a 24-hr acclimation period. Heat production, total carbon dioxide production and oxygen consumption, and RER were determined by Comprehensive laboratory animal monitoring system (CLAMS).

Insulin Tolerance test (ITT) and Glucose Tolerance test (GTT)

For ITT, male mice fasted for 4 h and received an intraperitoneal injection of human insulin (0.75 IU/kg). For GTT, male mice fasted for 16 h received an intraperitoneal

injection of glucose (1 g/kg). A series of blood glucose concentrations were measured from tail blood at the indicated times using a One-Touch Ultra® glucometer (LifeScan Inc., Milpitas, CA).

Chromatin Immunoprecipitation (ChIP)

The ChIP assay was performed using Sonication ChIP Kit (Abclonal, Cat#RK20258). Briefly, the liver tissues or primary hepatocytes were collected and cross-linking fixed. Cross-linked chromatin fragments were precipitated with Rabbit control IgG (Abclonal, Cat#AC005) or anti-H3K27me3 antibody (Abclonal, Cat# A16199) for subsequent PCR analysis using the amplification primers for mouse PPARγ promoter (+101~+420bp), TATTGGGTCGCGCGCAGCC and ACACAGTCCTGTCAGAACG.

RNA immunoprecipitation (RIP)

The RIP assay was performed using RIP Assay Kit (BersinBio, Cat#Bes5101). Briefly, heap 1-6 cells were transfected by indicated plasmids, respectively. The cells were collected, cross-linking fixed and precipitated with Mouse Control IgG (Abclonal, Cat#AC011) or anti-FLAG antibody (Abclonal, Cat#AE005) for subsequent RT-qPCR analysis using the amplification primers for *Snhg3*.

RNA sequencing (RNA-Seq)

The RNA-Seq was performed according to the manufacturer's protocol (BGI-Shenzhen, https://www.yuque.com/yangyulan-ayaeq/oupzan/fuoao4). Briefly, total RNA was extracted from liver of 3 male DIO (27 weeks) mice and 3 male control mice for RNA-Seq to screen the differentially expressed lncRNAs using Trizol (Invitrogen, Carlsbad, CA, USA) according to manual instruction. rRNA in total RNA removed using RNase H kit, was subsequently to construct library and perform sequencing analysis. The data were mapped to mouse genome (GRCm39) by using Bowtie2. The data for the differentially expressed lncRNAs had been deposited to National Genomics Data Center, China National Center for Bioinformation (NGDC-CNCB) (https://ngdc.cncb.ac.cn/) with the dataset identifier CRA009822. Additionally, total RNA was extracted from livers of 3 male DIO *Snhg3*-HKI mice and 3 male DIO WT mice for RNA-Seq to screen the differentially expressed mRNAs

using Trizol. Total RNA was enriched by oligo (dT)-attached magnetic beads, followed by library construction and sequencing analysis. The data were mapped to mouse genome (GRCm39) by using Bowtie2. The data for the differentially expressed mRNAs have been deposited to the Sequence Read Archive (SRA) (submit.ncbi.nlm.nih.gov) with the dataset identifier PRJNA904058.

Assay for Transposase-Accessible Chromatin with high throughput sequencing (ATAC-Seq)

The ATAC-seq was performed according to manufacturer's protocols (BGI_Shenzhen, https://www.yuque.com/yangyulan-ayaeq/oupzan/lllmzg). Briefly, fresh liver tissue samples from 3 male DIO *Snhg3*-HKI mice and 3 male DIO control mice were flash frozen by liquid nitrogen and then ground completely. The transposition reactions were initiated by adding transposase. The PCR reaction system was configured to initiate PCR amplification of the transposition products. The corresponding library quality control protocol would be selected depending on product requirements. Single-stranded PCR products were produced via denaturation. The reaction system and program for circularization were subsequently configured and set up. Single-stranded cyclized products were produced, while uncyclized linear DNA molecules were digested. Single-stranded circle DNA molecules were replicated via rolling cycle amplification, and a DNA nanoball (DNB) which contain multiple copies of DNA was generated. Sufficient quality DNBs were then loaded into patterned nanoarrays using high-intensity DNA nanochip technique and sequenced through combinatorial Probe-Anchor Synthesis (cPAS). Data were filtered by removing adaptor sequences, contamination and low-quality reads from raw reads. Bowtie2 was used to do genome alignment after evaluating its performance.

Peak Calling was performed by MACS (Model-based Analysis for ChIP-Seq). The candidate Peak region was extended to be long enough for modeling. Dynamic Possion Distribution was used to calculate the p-value of the specific region based on the unique mapped reads. The region would be defined as a Peak when the p-value < 1e-05. MACS works well for the identification of the sharp peaks of most sequence-specific transcription factors.

Peak Distribution On Gene Elements. Peaks were classified based on the location (UCSC annotation data) and showed in the following genome regions: promoter (<=1kb), promoter (1−2kb), promoter (2−3kb), 5'-UTR, 3'-UTR, intergenic, introns, and exons.

Differential Peaks were identified using MAnorm. First, the true intensities of the most common peaks were assumed to be the same between two ATAC-Seq samples. Second, the observed differences in sequence read density in common peaks were presumed to reflect the scaling relationship of ATAC-Seq signals between two samples, which could thus be applied to all peaks. Based on these hypotheses, the log2 ratio of read density between two samples M was plotted against the average log2 read density A for all peaks, and robust linear regression was applied to fit the global dependence between the M-A values of common peaks. Then the derived linear model was used as a reference for normalization and extrapolated to all peaks. Finally, the p-value for each Peak was calculated based on the Bayesian model, the significant regions were picked up if |M=log2FC| > 2 and p-value < 0.001. To identify differentially expressed genes (DARs), the count matrix was input into MAnorm with the cutoff of abs(log2FC)>2 and p-value<0.001. Genomic features of DARs were annotated by R package ChIPseeker (v1.30.3).

Differential motifs analysis. After extracting the corresponding peak sequence, Hypergeometric Optimization of Motif EnRichment (HOMER, Homer Software and Data Download (ucsd.edu)) and Cis-Regulatory Element Motif Activities (CREMA - Cis-Regulatory Element Motif Analysis (unibas.ch)) were used for motif analysis. Genomic regions with differential ATAC peaks were shown using IGV software.

The data of ATAC-seq has been deposited to National Genomics Data Center, China National Center for Bioinformation (NGDC-CNCB) (https://ngdc.cncb.ac.cn/) with the dataset identifier CRA009511.

Integrated analysis ATAC-Seq data with RNA-Seq data

The common number and unique number of genes associated with DARs and DEGs were counted using Wayne comparative analysis. The values of each quadrant satisfying the log2FC condition were selected from DARs-associated genes and DEGs

respectively to draw a nine-quadrant plot. Pearson correlation was calculated for both sets of data and p-value was calculated using the Z-test.

Cleavage Under Targets and Tagmentation sequencing (CUT&Tag-Seq)

CUT&Tag was performed according to the Hyperactive Universal CUT&Tag Assay Kit for Illumina (Vazyme, Nanjing, Cat#TD903-01). Briefly, the mixed liver tissues from 3 DIO *Snhg3*-HKO mice were used for the CUT&Tag experiment. pA-Tn5 transposase was used to cut the genome and add a special adaptor sequence to build a library. The single-stranded PCR products were sequenced on illumina/DNBSEQ-T7 platform PE150 (Annoroad Gene Technology Co.ltd). The data were mapped to mouse genome (GRCm38) by using Bowtie2. Genomic features of DARs were annotated by R package ChIPseeker (v1.30.3). The data of Cut&Tag has been deposited to National Genomics Data Center, China National Center for Bioinformation (NGDC-CNCB) (https://ngdc.cncb.ac.cn/) with the dataset identifier CRA009582.

Biotin-RNA pull-down and mass spectrometry assay

Biotin-RNA pull-down assay was performed as described in a previous study***(Guo, Zhao et al., 2018***). Briefly, *Snhg3* DNA was amplified from mouse liver cDNA using the primers listed in the Table 1 and lacZ DNA fragment were constructed into pGEM-T easy vector. The pGEM-T-*Snhg3* and pGEM-T-lacZ vectors were linearized by restriction enzyme digestion, then transcribed to *Snhg3* and lacZ fragments. Biotinylated RNAs were transcribed in vitro with Biotin-RNA Labeling Mix (Roche, Indianapolis, IN) and purified with quick spin RNA columns (Roche, Indianapolis, IN). Biotin-labeled RNA or unbiotinylated RNAs was dissolved in RNA structure buffer (10 mM Tris, pH 7.0, 0.1 M KCl, 10 mM MgCl2) to allow formation of the secondary structure. Primary hepatocytes lysates were added to biotin-labeled RNA or unbiotinylated RNA. Streptavidin agarose beads (GE Healthcare, Little Chalfont, UK) were mixed with a pull-down reaction and then rotated constantly. RNA affinity captures were subjected to 12% SDS-PAGE followed by coomassie blue staining or Western blotting. The various bands that were visualized by coomassie blue staining were excised and subjected to mass spectrometry analyses (LC-MS/MS, A TripleTOF ®, ABsciex, Concord, ON). The data of RNA pull-down for *Snhg3*, control or lacZ

were deposited to the iProX (https://www.iprox.cn/) with the dataset identifier PXD039526.

Ubiquitination assays

For endogenous ubiquitination assays, Hepa1-6 cells were transfected with the indicated combinations of plasmids, including HA-ubiquitin and *Snhg3* plasmids. For exogenous ubiquitination assays, Hepa1-6 cells were transfected with the indicated combinations of plasmids, including HA-ubiquitin, HA-K33-ubiquitin, HA-K63-ubiquitin, HA-K48-ubiquitin, Flag-SND1 and *Snhg3* plasmids. Cells were treated with 20 μM MG132 proteasome inhibitor (M1902, AbMole) for 6 hours prior to lyse in lysis buffer (200 mM NaCl, 20 mM Tris-HCl (pH 7.4), 2.5 mM MgCl2, 0.5% Triton X-100, 1 mM PMSF, and protease inhibitor cocktail and then were sonicated. After centrifugation at 14,000 g, the cleared lysates were subjected to immunoprecipitation with anti-SND1 antibody (sc-166676, Santa Cruz) for endogenous ubiquitination assays or with anti-DDDDK-tag magnetic beads (M185-10R, MBL) for exogenous ubiquitination assays. The immunocomplexes were collected and subjected to Western blotting with the indicated antibodies.

Statistical analysis

Data analyses were performed with SPSS (Version 17.0, SPSS, Inc.). The curves of body weight and ITT were analyzed using a repeated measure two-way ANOVA. For the other statistical analysis, the Kolmogorov-Smirnov test was firstly used for normality test. For the data conforming to the normal distribution, experiments were analyzed using Independent-Samples T-test or one-way ANOVA. All data were presented as the mean ± SD or the mean ± SEM. * $p < 0.05$ was considered statistically significant.

Acknowledgments

This work was supported by Chinese Academy of Medical Sciences Innovation Fund for Medical Sciences (CIFMS2021-I2M-1-016) and National Key R&D Program of China (2022YFC2504002, 2022YFC2504003). We thank Dr. Yi Li (Cancer Hospital, Chinese Academy of Medical

Sciences and Peking Union Medical College) for providing the plasmid of HA-Ub, HA-Ub-K63 and HA-Ub-K48. We thank Cyagen Biosciences for the collaborative efforts in the creation of *Snhg3*-loxP and liver-specific knock-in *Snhg3* mice. We thank BGI-Shenzhen for the collaborative efforts in RNA-Seq and ATAC-Seq technology. We thank Anoroad gene technology (Beijing) for the collaborative efforts in Cut&Tag-Seq and Jingjie PTM BioLab (Hangzhou) Co. Ltd for the collaborative efforts in mass spectrometry technology resources.

Author Contributions

Xianghong Xie performed all experiments, acquired and analyzed the data, generated the figures and wrote the manuscript. Mingyue Gao, Wei Zhao, Chunmei Li, Weihong Zhang, Jiahui Yang, Yinliang Zhang, Enhui Chen, Yanfang Guo, Zeyu Guo, Minglong Zhang, Yinghan Zhu, Yiting Wang and Xiaolu Li performed experiments, acquired and analyzed the data. Ebenezeri Erasto Ngowi revised the manuscript. Heping Wang and Xiaoman Wang analyzed the data and generated the figures. Hong Yao, Li Yan and Fude Fang provided additional reagents and revised the manuscript. Meixia Li, Aijun Qiao and Xiaojun Liu devised and supervised the experimental plan and edited the manuscript.

Conflicts of Interest

The author(s) declare(s) that there is no conflict of interest regarding the publication of this article.

Data Availability

All data generated and analysed that support the findings of this study are available from the corresponding author upon reasonable request. The lncRNA-Seq data had been deposited to National Genomics Data Center, China National Center for Bioinformation (NGDC-CNCB) (https://ngdc.cncb.ac.cn/) with the dataset identifier CRA009822. The data of RNA pull-down for *Snhg3*, control or lacZ have been deposited to the iProX (https://www.iprox.cn/) with the dataset identifier PXD039526. The data of RNA-seq have been deposited to the Sequence Read Archive (SRA) with

the dataset identifier PRJNA904058. The data of ATAC-seq and Cut&Tag have been deposited to National Genomics Data Center, China National Center for Bioinformation (NGDC-CNCB) (https://ngdc.cncb.ac.cn/) with the dataset identifier CRA009511 and CRA009582, respectively.

Supplementary Materials

Table S1 to S10.

References

Ackermann AM, Wang Z, Schug J, Naji A, Kaestner KH. 2016. Integration of ATAC-seq and RNA-seq identifies human alpha cell and beta cell signature genes. *Molecular Metabolism* **5**: 233-244. DOI: 10.1016/j.molmet.2016.01.002, PMID: 26977395

Baffy G. 2015. MicroRNAs in Nonalcoholic Fatty Liver Disease. *Journal of Clinical Medicine* **4**: 1977-1988. DOI: 10.3390/jcm4121953, PMID: 26690233

Bayoumi A, Gronbaek H, George J, Eslam M. 2020. The Epigenetic Drug Discovery Landscape for Metabolic-associated Fatty Liver Disease. *Trends In Genetics* **36**: 429-441. DOI: 10.1016/j.tig.2020.03.003, PMID: 32396836

Briata P, Gherzi R. 2020. Long Non-Coding RNA-Ribonucleoprotein Networks in the Post-Transcriptional Control of Gene Expression. *Noncoding RNA* **6**:40. DOI: 10.3390/ncrna6030040, PMID: 32957640

Buzzetti E, Pinzani M, Tsochatzis EA. 2016. The multiple-hit pathogenesis of non-alcoholic fatty liver disease (NAFLD). *Metabolism* **65**: 1038-1048. DOI: 10.1016/j.metabol.2015.12.012, PMID: 26823198

Byun S, Seok S, Kim YC, Zhang Y, Yau P, Iwamori N, Xu HE, Ma J, Kemper B, Kemper JK. 2020. Fasting-induced FGF21 signaling activates hepatic autophagy and lipid degradation via JMJD3 histone demethylase. *Nature Communications* **11**: 807. DOI: 10.1038/s41467-020-14384-z, PMID: 32042044

Chen ZJ, Pikaard CS. 1997. Epigenetic silencing of RNA polymerase I transcription: a role for DNA methylation and histone modification in nucleolar dominance. *Genes & Development* **11**: 2124-2136. DOI: 10.1101/gad.11.16.2124, PMID: 9284051

Duan Z, Zhao X, Fu X, Su C, Xin L, Saarikettu J, Yang X, Yao Z, Silvennoinen O, Wei M, Yang J. 2014. Tudor-SN, a novel coactivator of peroxisome proliferator-activated receptor gamma protein, is essential for adipogenesis. *Journal of Biological Chemistry* **289**: 8364-8374. DOI: 10.1074/jbc.M113.523456, PMID: 24523408

741 **Eslam M**, Valenti L, Romeo S. 2018. Genetics and epigenetics of NAFLD and NASH: Clinical
742 impact. *Journal of Hepatology* **68**: 268-279. DOI: 10.1016/j.jhep.2017.09.003, PMID:
743 29122391
744 **Friedman SL**, Neuschwander-Tetri BA, Rinella M, Sanyal AJ. 2018. Mechanisms of NAFLD
745 development and therapeutic strategies. *Nature Medicine* **24**: 908-922. DOI:
746 10.1038/s41591-018-0104-9, PMID: 29967350
747 **Gavrilova O**, Haluzik M, Matsusue K, Cutson JJ, Johnson L, Dietz KR, Nicol CJ, Vinson C,
748 Gonzalez FJ, Reitman ML. 2003. Liver peroxisome proliferator-activated receptor gamma
749 contributes to hepatic steatosis, triglyceride clearance, and regulation of body fat mass.
750 *Journal of Biological Chemistry* **278**: 34268-34276. DOI: 10.1074/jbc.M300043200, PMID:
751 12805374
752 **Gofton C**, Upendran Y, Zheng MH, George J. 2023. MAFLD: How is it different from NAFLD?
753 *Clinical and Molecular Hepatology* **29**: S17-S31. DOI: 10.3350/cmh.2022.0367, PMID:
754 36443926
755 **Guo H**, Zhao L, Shi B, Bao J, Zheng D, Zhou B, Shi J. 2018. GALNT5 uaRNA promotes gastric
756 cancer progression through its interaction with HSP90. *Oncogene* **37**: 4505-4517. DOI:
757 10.1038/s41388-018-0266-4, PMID: 29743591
758 **Jonas W**, Schurmann A. 2021. Genetic and epigenetic factors determining NAFLD risk.
759 *Molecular Metabolism* **50**: 101111. DOI: 10.1016/j.molmet.2020.101111, PMID: 33160101
760 **Jun HJ**, Kim J, Hoang MH, Lee SJ. 2012. Hepatic lipid accumulation alters global histone h3
761 lysine 9 and 4 trimethylation in the peroxisome proliferator-activated receptor alpha
762 network. *PLoS One* **7**: e44345. DOI: 10.1371/journal.pone.0044345, PMID: 22973438
763 **Kang YJ**, Yang DC, Kong L, Hou M, Meng YQ, Wei L, Gao G. 2017. CPC2: a fast and accurate
764 coding potential calculator based on sequence intrinsic features. *Nucleic Acids Research* **45**:
765 W12-W16. DOI: 10.1093/nar/gkx428, PMID: 28521017
766 **Karri K**, Waxman DJ. 2023. Dysregulation of murine long noncoding single-cell transcriptome
767 in nonalcoholic steatohepatitis and liver fibrosis. *RNA* **29**: 977-1006. DOI:
768 10.1261/rna.079580.123, PMID: 37015806
769 **Koonen DP**, Jacobs RL, Febbraio M, Young ME, Soltys CL, Ong H, Vance DE, Dyck JR. 2007.
770 Increased hepatic CD36 expression contributes to dyslipidemia associated with diet-induced
771 obesity. *Diabetes* **56**: 2863-2871. DOI: 10.2337/db07-0907, PMID: 17728375
772 **Lee J**, Kim Y, Friso S, Choi SW. 2017. Epigenetics in non-alcoholic fatty liver disease.
773 *Molecular Aspects of Medicine* **54**: 78-88. DOI: 10.1016/j.mam.2016.11.008, PMID:
774 27889327
775 **Lee SM**, Muratalla J, Karimi S, Diaz-Ruiz A, Frutos MD, Guzman G, Ramos-Molina B,
776 Cordoba-Chacon J. 2023. Hepatocyte PPARgamma contributes to the progression of
777 non-alcoholic steatohepatitis in male and female obese mice. *Cellular And Molecular Life*
778 *Sciences* **80**: 39. DOI: 10.1007/s00018-022-04629-z, PMID: 36629912
779 **Lee SM**, Muratalla J, Sierra-Cruz M, Cordoba-Chacon J. 2023. Role of hepatic peroxisome
780 proliferator-activated receptor gamma in non-alcoholic fatty liver disease. *Journal of*
781 *Endocrinology* **257**: e220155. DOI: 10.1530/JOE-22-0155, PMID: 36688873
782 **Lee SM**, Pusec CM, Norris GH, De Jesus A, Diaz-Ruiz A, Muratalla J, Sarmento-Cabral A,
783 Guzman G, Layden BT, Cordoba-Chacon J. 2021. Hepatocyte-Specific Loss of PPARgamma
784 Protects Mice From NASH and Increases the Therapeutic Effects of Rosiglitazone in the Liver.

785 *Cellular and Molecular Gastroenterology and Hepatology* **11**: 1291-1311. DOI:
786 10.1016/j.jcmgh.2021.01.003, PMID: 33444819
787 **Lee YK**, Park JE, Lee M, Hardwick JP. 2018. Hepatic lipid homeostasis by peroxisome
788 proliferator-activated receptor gamma 2. *Liver Research* **2**: 209-215. DOI:
789 10.1016/j.livres.2018.12.001, PMID: 31245168
790 **Loomba R**, Friedman SL, Shulman GI. 2021 Mechanisms and disease consequences of
791 nonalcoholic fatty liver disease. *Cell* **184**: 2537-2564. DOI: 10.1016/j.cell.2021.04.015, PMID:
792 33989548
793 **Mann DA**. 2014. Epigenetics in liver disease. *Hepatology* **60**: 1418-1425. DOI:
794 10.1002/hep.27131, PMID: 24633972
795 **Matsumoto M**, Ogawa W, Teshigawara K, Inoue H, Miyake K, Sakaue H, Kasuga M. 2002.
796 Role of the insulin receptor substrate 1 and phosphatidylinositol 3-kinase signaling pathway
797 in insulin-induced expression of sterol regulatory element binding protein 1c and
798 glucokinase genes in rat hepatocytes. *Diabetes* **51**: 1672-1680. DOI:
799 10.2337/diabetes.51.6.1672, PMID: 12031952
800 **Matsusue K**, Kusakabe T, Noguchi T, Takiguchi S, Suzuki T, Yamano S, Gonzalez FJ. 2008.
801 Hepatic steatosis in leptin-deficient mice is promoted by the PPARgamma target gene Fsp27.
802 *Cell Metabolism* **7**: 302-11. DOI: 10.1016/j.cmet.2008.03.003, PMID: 18396136
803 **Medina-Gomez G**, Gray SL, Yetukuri L, Shimomura K, Virtue S, Campbell M, Curtis RK,
804 Jimenez-Linan M, Blount M, Yeo GS, Lopez M, Seppanen-Laakso T, Ashcroft FM, Oresic M,
805 Vidal-Puig A. 2007. PPAR gamma 2 prevents lipotoxicity by controlling adipose tissue
806 expandability and peripheral lipid metabolism. *PLoS Genetics* **3**: e64. DOI:
807 10.1371/journal.pgen.0030064, PMID: 17465682
808 **Morey C**, Avner P. 2004. Employment opportunities for non-coding RNAs. *FEBS Letters* **567**:
809 27-34. DOI: 10.1016/j.febslet.2004.03.117, PMID: 15165889
810 **Mukherjee AG**, Wanjari UR, Gopalakrishnan AV, Katturajan R, Kannampuzha S, Murali R,
811 Namachivayam A, Ganesan R, Renu K, Dey A, Vellingiri B, Prince SE. 2022. Exploring the
812 Regulatory Role of ncRNA in NAFLD: A Particular Focus on PPARs. *Cells* **11**:3959. DOI:
813 10.3390/cells11243959, PMID: 36552725
814 **Navarro-Imaz H**, Ochoa B, Garcia-Arcos I, Martinez MJ, Chico Y, Fresnedo O, Rueda Y. 2020.
815 Molecular and cellular insights into the role of SND1 in lipid metabolism. *Biochimica Et*
816 *Biophysica Acta- Molecular and Cell Biology of Lipids* **1865**: 158589. DOI:
817 10.1016/j.bbalip.2019.158589, PMID: 31978555
818 **Ng SY**, Lin L, Soh BS, Stanton LW. 2013. Long noncoding RNAs in development and disease of
819 the central nervous system. *Trends in genetics* 29: 461-468. DOI: 10.1016/j.tig.2013.03.002,
820 PMID: 23562612
821 **Peixoto P**, Cartron PF, Serandour AA, Hervouet E. 2020. From 1957 to Nowadays: A Brief
822 History of Epigenetics. *International Journal of Molecular Sciences* **21**:7571. DOI:
823 10.3390/ijms21207571, PMID: 33066397
824 **Pirola CJ**, Sookoian S. 2020. Epigenetics factors in nonalcoholic fatty liver disease. *Expert*
825 *Review of Gastroenterology & Hepatology* **16**:521-536. DOI:
826 10.1080/17474124.2020.1765772, PMID: 32476509

Rada P, Gonzalez-Rodriguez A, Garcia-Monzon C, Valverde AM. 2020. Understanding lipotoxicity in NAFLD pathogenesis: is CD36 a key driver? *Cell Death & Disease* **11**: 802. DOI: 10.1038/s41419-020-03003-w, PMID: 32978374

Rinella ME, Lazarus JV, Ratziu V, Francque SM, Sanyal AJ, Kanwal F, Romero D, Abdelmalek MF, Anstee QM, Arab JP, Arrese M, Bataller R, Beuers U, Boursier J, Bugianesi E, Byrne CD, Castro Narro GE, Chowdhury A, Cortez-Pinto H, Cryer DR, Cusi K, El-Kassas M, Klein S, Eskridge W, Fan J, Gawrieh S, Guy CD, Harrison SA, Kim SU, Koot BG, Korenjak M, Kowdley KV, Lacaille F, Loomba R, Mitchell-Thain R, Morgan TR, Powell EE, Roden M, Romero-Gómez M, Silva M, Singh SP, Sookoian SC, Spearman CW, Tiniakos D, Valenti L, Vos MB, Wong VW, Xanthakos S, Yilmaz Y, Younossi Z, Hobbs A, Villota-Rivas M, Newsome PN; NAFLD Nomenclature consensus group. 2023. A multisociety Delphi consensus statement on new fatty liver disease nomenclature. *Hepatology* **78**: 1966-1986. DOI: 10.1097/HEP.0000000000000520, PMID: 37363821

Ruan X, Li P, Ma Y, Jiang CF, Chen Y, Shi Y, Gupta N, Seifuddin F, Pirooznia M, Ohnishi Y, Yoneda N, Nishiwaki M, Dumbovic G, Rinn JL, Higuchi Y, Kawai K, Suemizu H, Cao H. 2021. Identification of human long noncoding RNAs associated with nonalcoholic fatty liver disease and metabolic homeostasis. *Journal of Clinical Investigation* **131**: e136336. DOI: 10.1172/JCI136336, PMID: 33048844

Sakurai Y, Kubota N, Yamauchi T, Kadowaki T. 2021. Role of Insulin Resistance in MAFLD. *International Journal of Molecular Sciences* **22** :4156. DOI: 10.3390/ijms22084156, PMID: 33923817

Sans A, Bonnafous S, Rousseau D, Patouraux S, Canivet CM, Leclere PS, Tran-Van-Nhieu J, Luci C, Bailly-Maitre B, Xu X, Lee AH, Minehira K, Anty R, Tran A, Iannelli A, Gual P. 2019. The Differential Expression of Cide Family Members is Associated with Nafld Progression from Steatosis to Steatohepatitis. *Scientific Reports* **9**: 7501. DOI: 10.1038/s41598-019-43928-7, PMID: 31097771

Sen R, Fallmann J, Walter M, Stadler PF. 2020. Are spliced ncRNA host genes distinct classes of lncRNAs? *Theory In Biosciences* **139**: 349-359. DOI: 10.1007/s12064-020-00330-6, PMID: 33219910

Skat-Rordam J, Hojland Ipsen D, Lykkesfeldt J, Tveden-Nyborg P. 2019. A role of peroxisome proliferator-activated receptor gamma in non-alcoholic fatty liver disease. *Basic & Clinical Pharmacology & Toxicology* **124**: 528-537. DOI: 10.1111/bcpt.13190, PMID: 30561132

Sodum N, Kumar G, Bojja SL, Kumar N, Rao CM. 2021. Epigenetics in NAFLD/NASH: Targets and therapy. *Pharmacological Research* **167**: 105484. DOI: 10.1016/j.phrs.2021.105484, PMID: 33771699

Sommerauer C, Kutter C. 2022. Noncoding RNAs and RNA-binding proteins: emerging governors of liver physiology and metabolic diseases. *American Journal of Physiology - Cell Physiology* **323**: C1003-C1017. DOI: 10.1152/ajpcell.00232.2022, PMID: 35968891

Sun T, Liu Z, Yang Q. 2020. The role of ubiquitination and deubiquitination in cancer metabolism. *Molecular Cancer* **19**: 146. DOI: 10.1186/s12943-020-01262-x, PMID: 33004065

Tessarz P, Kouzarides T. 2014. Histone core modifications regulating nucleosome structure and dynamics. *Nature Reviews Molecular Cell Biology* **15**: 703-708. DOI: 10.1038/nrm3890, PMID: 25315270

Thomson DW, Dinger ME. 2016. Endogenous microRNA sponges: evidence and controversy. *Nature Reviews Genetics* **17**: 272-283. DOI: 10.1038/nrg.2016.20, PMID: 27040487

Ulitsky I, Bartel DP. 2013. lincRNAs: genomics, evolution, and mechanisms. *Cell* **154**: 26-46. DOI: 10.1016/j.cell.2013.06.020, PMID: 23827673

Ying M, Chen D. 2012. Tudor domain-containing proteins of *Drosophila melanogaster*. *Development Growth & Differentiation* **54**: 32-43. DOI: 10.1111/j.1440-169x.2011.01308.x, PMID: 23741747

Zimta AA, Tigu AB, Braicu C, Stefan C, Ionescu C, Berindan-Neagoe I. 2020. An Emerging Class of Long Non-coding RNA With Oncogenic Role Arises From the snoRNA Host Genes. *Frontiers in Oncology* **10**: 389. DOI: 10.3389/fonc.2020.00389, PMID: 32318335

Figure legends

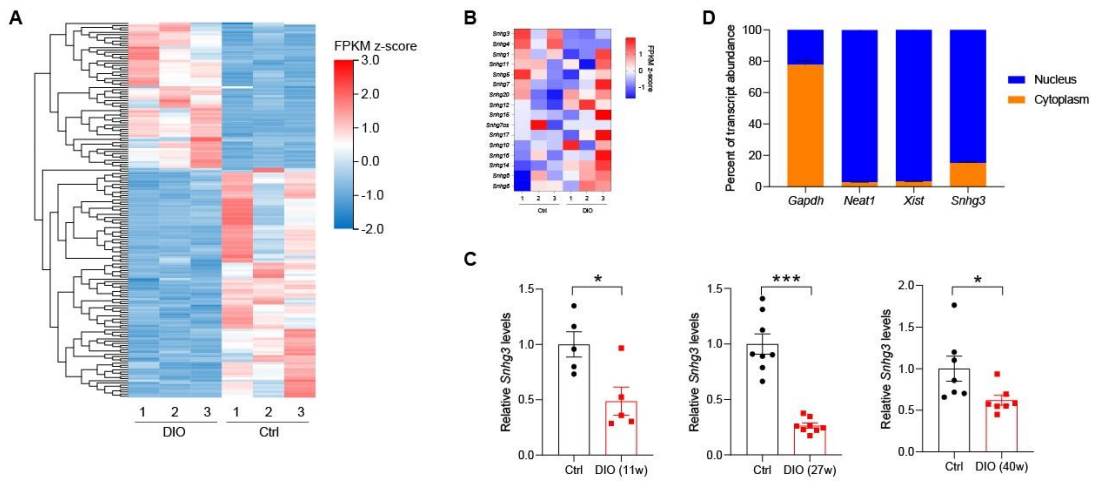

Figure 1. The expression of hepatic lncRNA-*Snhg3* is downregulated in high-fat diet-induced obesity mice. (**A**) Differentially expressed *lncRNAs* in livers of 6~8-week-old littermate male mice that were fed an HFD and control diet for 27 weeks (n = 3 mice/group). (**B**) Heat map of *Snhgs* in livers of mice as indicated in (**A**) (n = 3 mice/group). (**C**) Expression levels of *Snhg3* in the liver of 6~8-week-old littermate male mice that were fed an HFD and control diet for indicated time period 11, 27 and 40 weeks. (**D**) Relative *Snhg3* expression levels in nuclear and cytosolic fractions of mouse primary hepatocytes. Nuclear controls: *Neat1* and *Xist*; Cytosolic

control: *Gapdh*. Data are represented as mean ± SEM. *p < 0.05 and ***p < 0.001 by Student's t test.

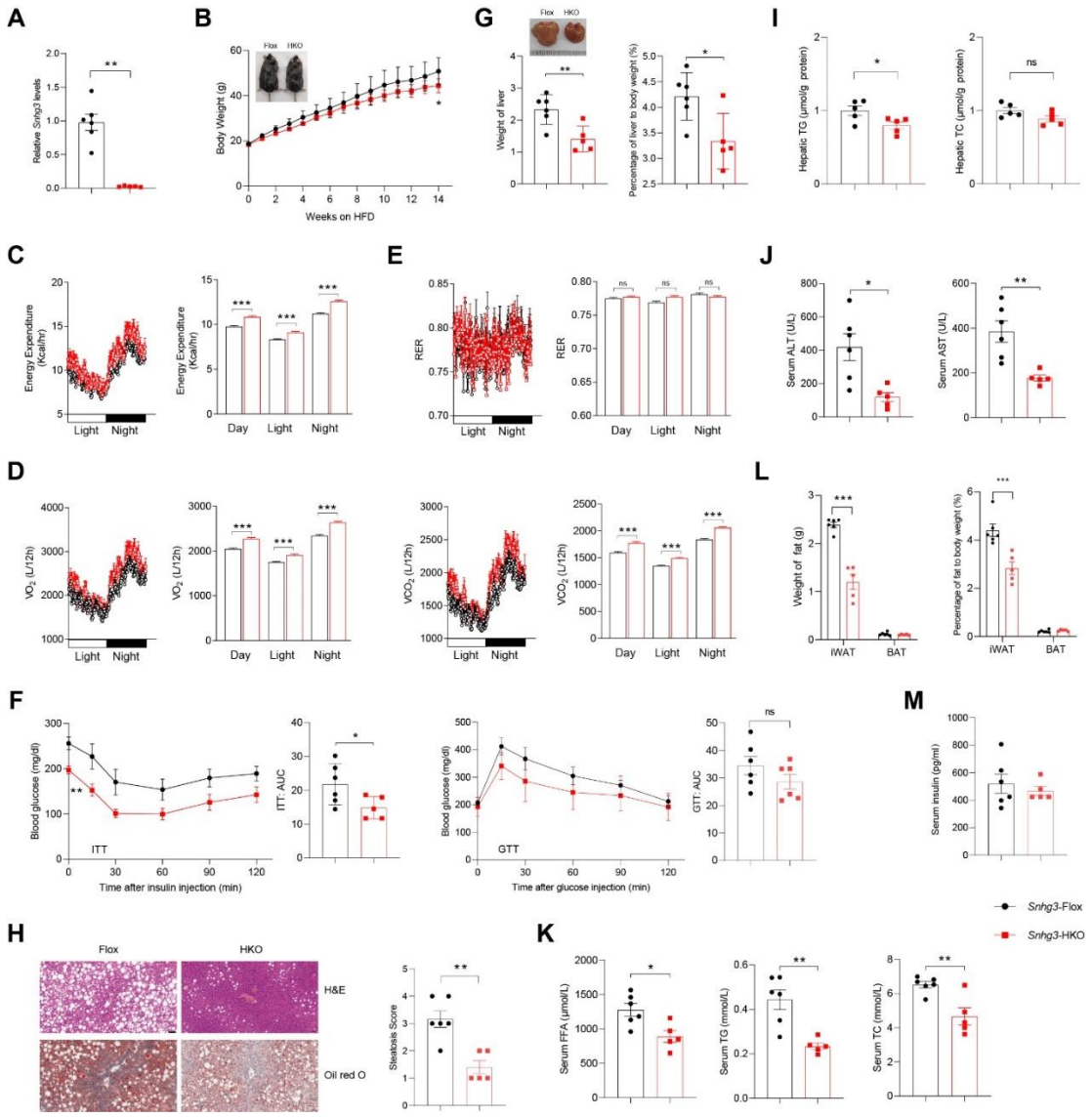

Figure 2. Liver specific *Snhg3* knockout improves high-fat diet-induced hepatic steatosis. (**A**) The expression of *Snhg3* was downregulated in the liver of *Snhg3*-HKO mice. n = 5/group. (**B**) Body weights of DIO *Snhg3*-Flox (n = 6) and *Snhg3*-HKO (n = 5) mice fed HFD for indicated time period. (**C - E**) Heat production (**C**), total oxygen consumption and carbon dioxide production (**D**), and RER (**E**) of DIO *Snhg3*-Flox (n = 6) and *Snhg3*-HKO (n = 5) mice fed HFD for 16 weeks were measured by CLAMS. (**F**) ITT and GTT of DIO *Snhg3*-Flox (n = 6) and *Snhg3*-HKO (n = 5) mice fed HFD for 18 weeks were analyzed, (AUC, Area Under Curve). (**G**) Liver weight (left) and

ratio (right) of liver weight/body weight of DIO *Snhg3*-Flox (n = 6) and *Snhg3*-HKO (n = 5) mice fed HFD for 21 weeks. (**H**) H&E and oil red O staining (left) and NASH score (right) of liver of DIO *Snhg3*-Flox and *Snhg3*-HKO mice as indicated in (**G**). Scare bars, 50 μm. (**I**) Hepatic TG and TC contents of mice as indicated in (**G**). (**J**) Serum ALT and AST concentrations of mice as indicated in (**G**). (**K**) Serum FFAs, TG and TG concentrations of mice as indicated in (**G**). (**L**) iWAT weight (left) and ratio (right) of iWAT weight/body weight of mice as indicated in (**G**). (**M**) Serum insulin concentration of mice as indicated in (**G**). Data are represented as mean ± SEM. *$p < 0.05$, **$p < 0.01$ and ***$p < 0.001$ by two-way ANOVA (**B** and **F**) and by Student's t test (the others).

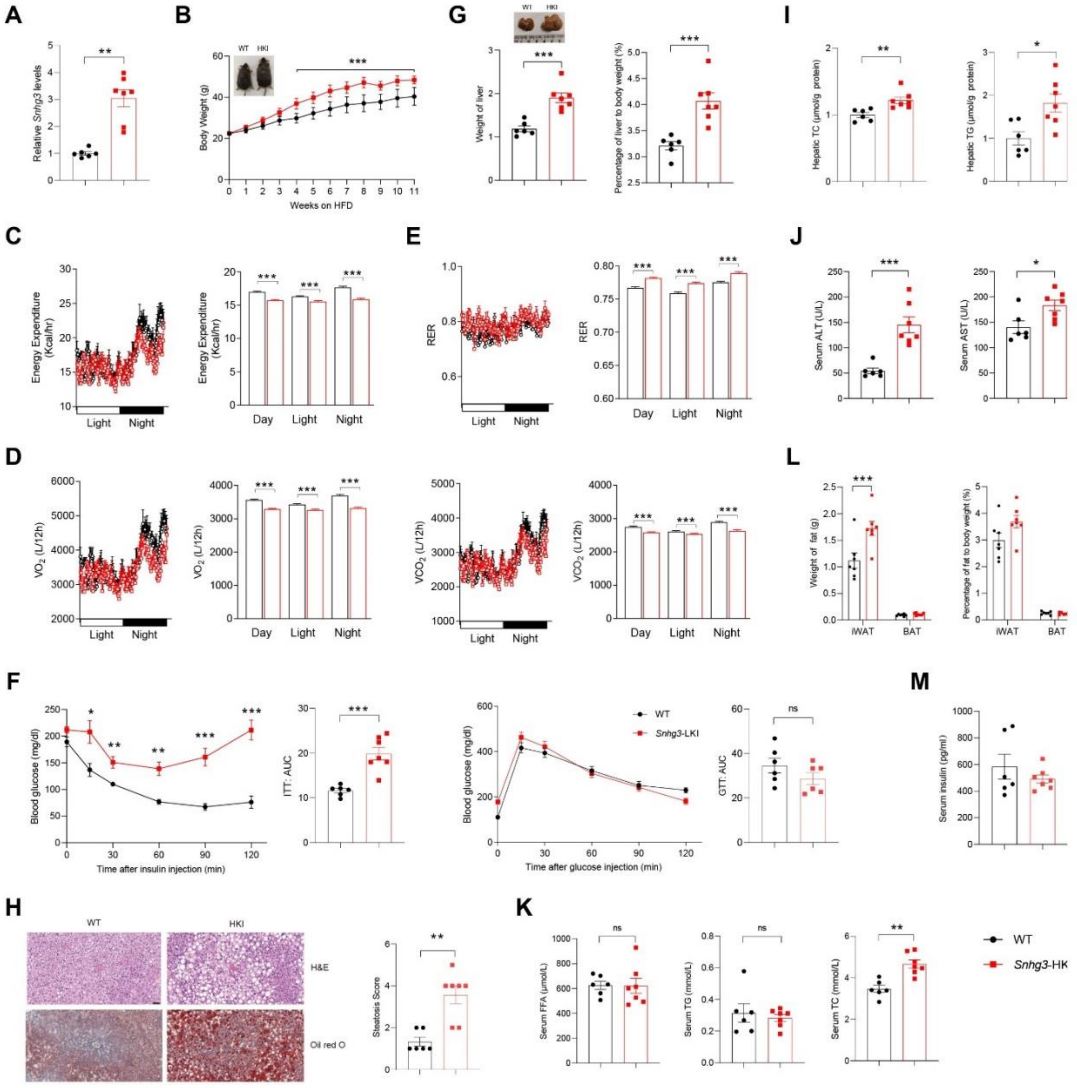

Figure 3. Liver specific *Snhg3* overexpression aggravates high-fat diet-induced hepatic steatosis. (**A**) The expression of *Snhg3* was upregulated in the liver of *Snhg3*-HKI mice. n = 7/group. (**B**) Body weights of DIO WT mice (n = 6) and *Snhg3*-HKI mice (n = 7) fed HFD for indicated times. (**C - E**), Heat production (**C**), total oxygen consumption and carbon dioxide production (**D**) and RER (**E**) of DIO WT (n = 6) and *Snhg3*-HKI (n = 7) mice fed HFD for 9 weeks were measured by CLAMS. (**F**) ITT and GTT of DIO WT (n = 6) and *Snhg3*-HKI (n = 7) mice fed HFD for 11 weeks were analyzed. (**G**) Liver weight (left) and ratio (right) of liver weight/body weight of DIO WT (n = 6) and *Snhg3*-HKI (n = 7) mice fed HFD for 13 weeks. (**H**) Liver H&E and oil red O staining (left) and NASH score (right) of DIO WT and *Snhg3*-HKI mice as indicated in (**G**). Scare bars, 50 μm. (**I**) Hepatic TG and

TC contents of mice as indicated in (**G**). (**J**) Serum ALT and AST concentrations of mice as indicated in (**G**). (**K**) Serum FFAs, TG and TG concentrations of mice as indicated in (**G**). (**L**) iWAT weight (left) and ratio (right) of iWAT weight/body weight of mice as indicated in (**G**). (**M**) Serum insulin concentration of mice as indicated in (**G**). Data are represented as mean ± SEM. *$p < 0.05$, **$p < 0.01$ and ***$p < 0.001$ by two-way ANOVA (**B** and **F**) and by Student's t test (the others).

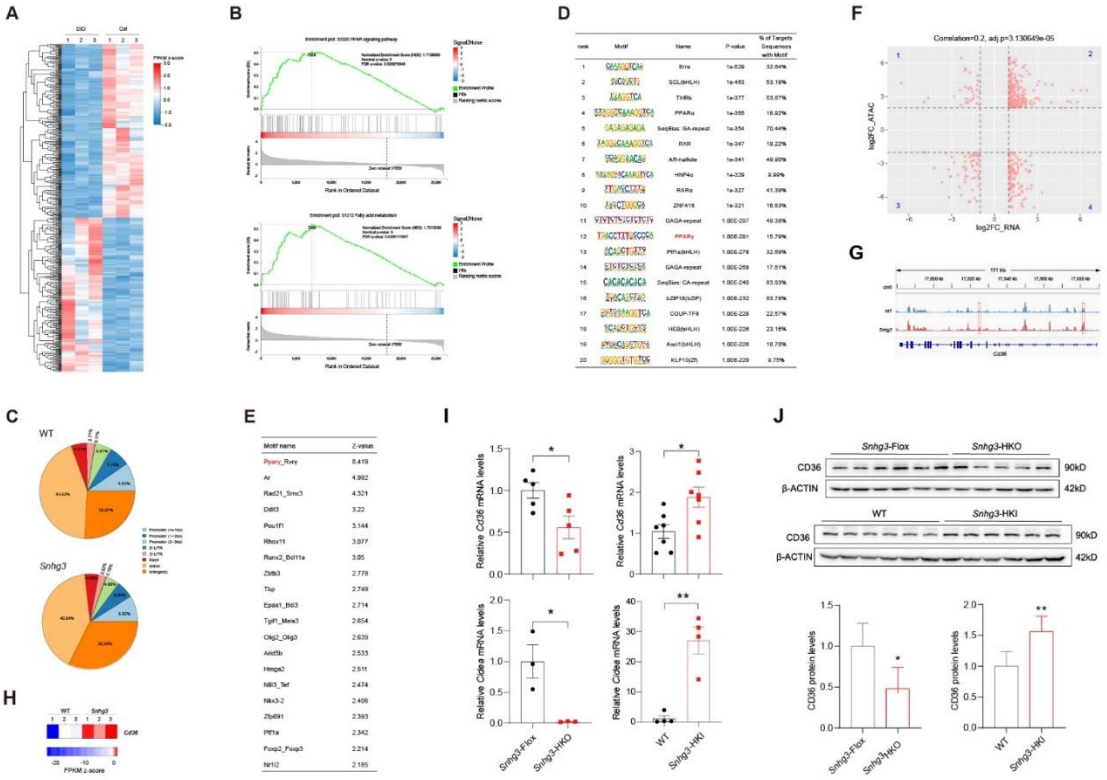

Figure 4. *Snhg3* promotes hepatic steatosis through regulating chromatin remodeling. (**A**) Differentially expressed genes in livers of DIO *Snhg3*-HKI and WT mice (n = 3 mice/group). (**B**) GSEA enrichment plot of PPAR signaling pathway set (KEGG pathway database) in livers of DIO *Snhg3*-HKI and WT mice (n = 3 mice/group). (**C**) Genome distribution ratio of the differentially accessible regions in the liver between DIO WT and DIO *Snhg3*-HKI mice by ATAC-Seq. (**D**) The transcription factors analysis in the accessible regions of the liver of DIO *Snhg3*-HKI mice by CREMA. (**E**) Integrated ATAC-Seq data with RNA-Seq data of DIO male mice and the control mice. (**F**) Chromatin accessibility at *Cd36* gene. (**G**) The heatmap of *Cd36* in livers of DIO male mice and the control mice (n = 3 mice/group). (**H** and **I**) Relative RNA (**H**) and protein (**I**, up, western blotting; down, quantitative result) levels of *Cd36* were measured in the liver. Data are represented as mean ± SD. *p < 0.05 and **p < 0.01 by Student's t test.

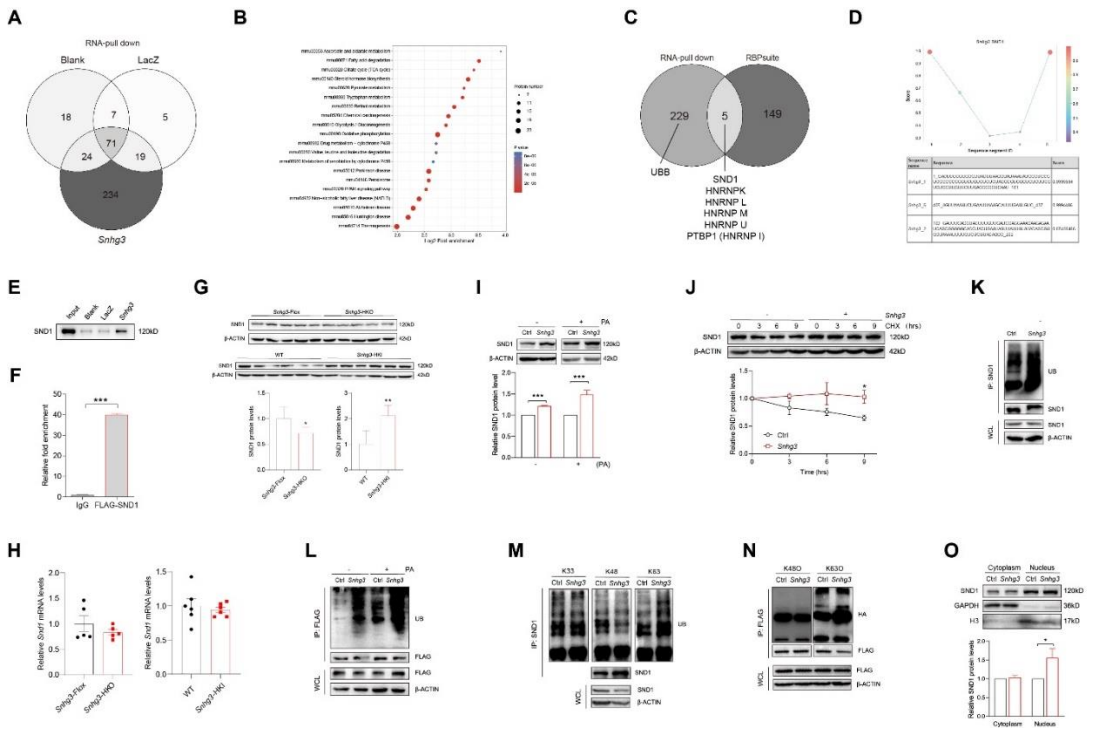

Figure 5. *Snhg3* induces SND1 expression and enhances the stability of SND1 protein through physiologically interacting with SND1. (**A**) Venn diagram of data from RNA pull-down & mass spectrometry (MS). (**B**) KEGG analysis of genes in specific *Snhg3*-binding proteins from RNA pull-down & MS. (**C**) Venn diagram of data from RNA pull-down & MS and bioinformatics predicted by RBPsuite (sjtu.edu.cn). (**D**) SND1 interacts with different fragments of *Snhg3* predicted by bioinformatics using RBPsuite (sjtu.edu.cn). (**E**) RNA pull-down & Western blotting confirms *Snhg3* interacting with SND1. (**F**) RIP confirms SND1 interacting with *Snhg3*. (**G** and **H**) Relative protein (**G**, up, western blotting; down, quantitative result) and RNA (**H**) levels of *Snd1* were measured in the liver. (**I**) *Snhg3* enhanced the protein level of SND1 in Hepa1-6 cells (up, western blotting; down, quantitative result). (**J**) *Snhg3* promoted the stability of SND1 protein in Hepa1-6 cells (up, western blotting; down, quantitative result). (**K** and **L**) *Snhg3* promoted the ubiquitination of endogenous (**K**) and exogenous (**L**) SND1 protein in Hepa1-6 cells. (**M** and **N**) *Snhg3* increased the K63-linked, not K48-linked and K33-linked, ubiquitination modification of endogenous (**M**) and exogenous (**N**) SND1 protein. o *Snhg3* induced the nuclear localization of SND1 in Hepa1-6 cells (up, western

blotting; down, quantitative result). Data are represented as mean ± SEM. *p < 0.05 and ***p < 0.001 by by two-way ANOVA (**J**) or Student's t test (the others).

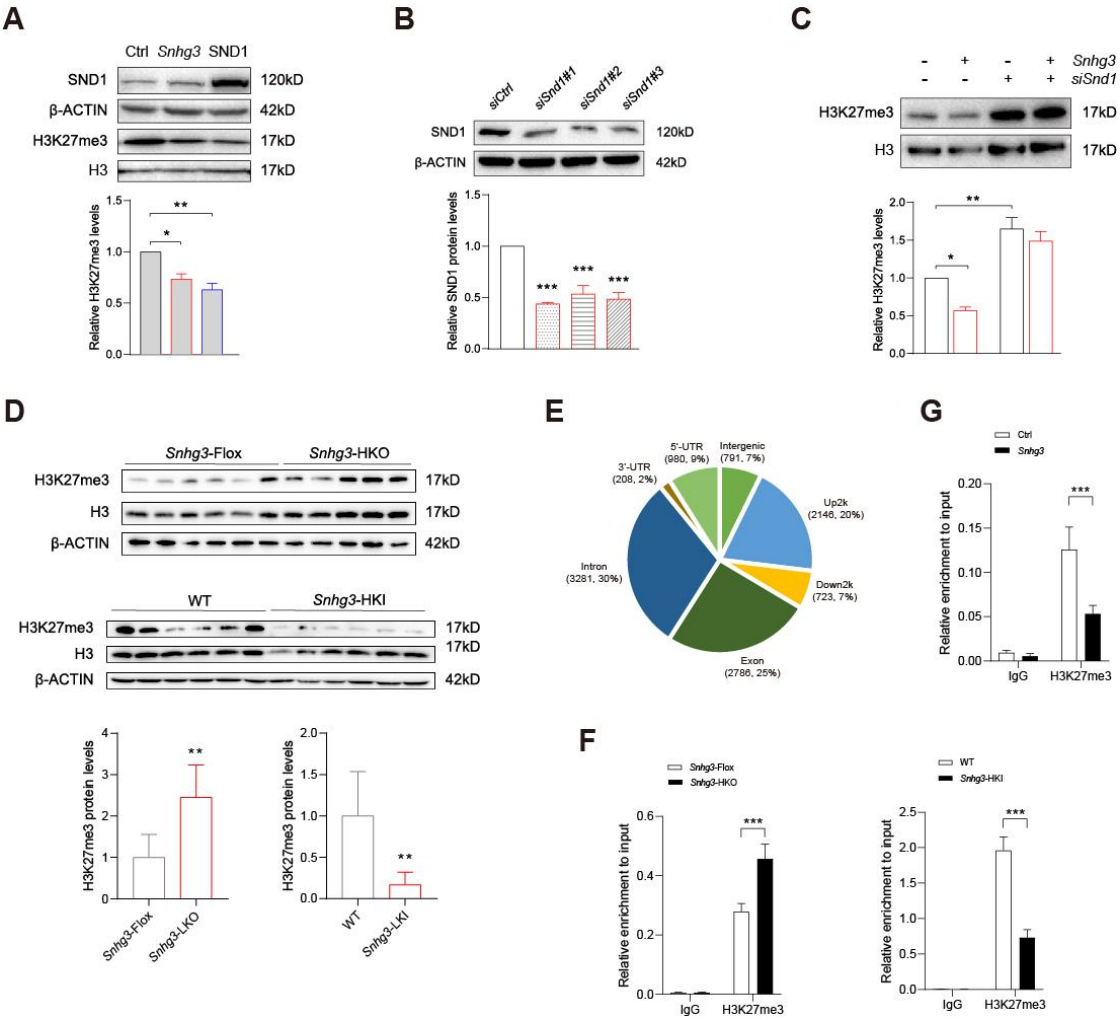

Figure 6. *Snhg3* increases PPARγ expression through reducing H3K27me3 enrichment at *Pparγ* promoter. (**A**) Overexpression of *Snhg3* or SND1 reduced the H3K27me3 level in Hepa1-6 cells with PA treatment (up, western blotting; down, quantitative result). (**B**) The expression of SND1 was disrupted with siRNA (up, western blotting; down, quantitative result). (**C**) Disruption SND1 expression reversed the *Snhg3*-induced decrease in H3K27me3 in primary hepatocytes (up, western blotting; down, quantitative result). (**D**) The H3K27me3 levels were measured in the liver of DIO *Snhg3*-HKO and *Snhg3*-HKI mice (up, western blotting; down, quantitative result). (**E**) Genome distribution ratio of H3K27me3 enrichment genetic sequence in the liver of DIO *Snhg3*-HKO mice. (**F** and **G**) ChIP result showed that *Snhg3* affected H3K27me3 enrichment at *Pparγ* promoter *in vivo* (**F**) and *in vitro* (**G**).

Data are represented as mean ± SEM. *p < 0.05, **p < 0.01 and ***p < 0.001 by one-way ANOVA (**C**) or by Student's t test (the others).

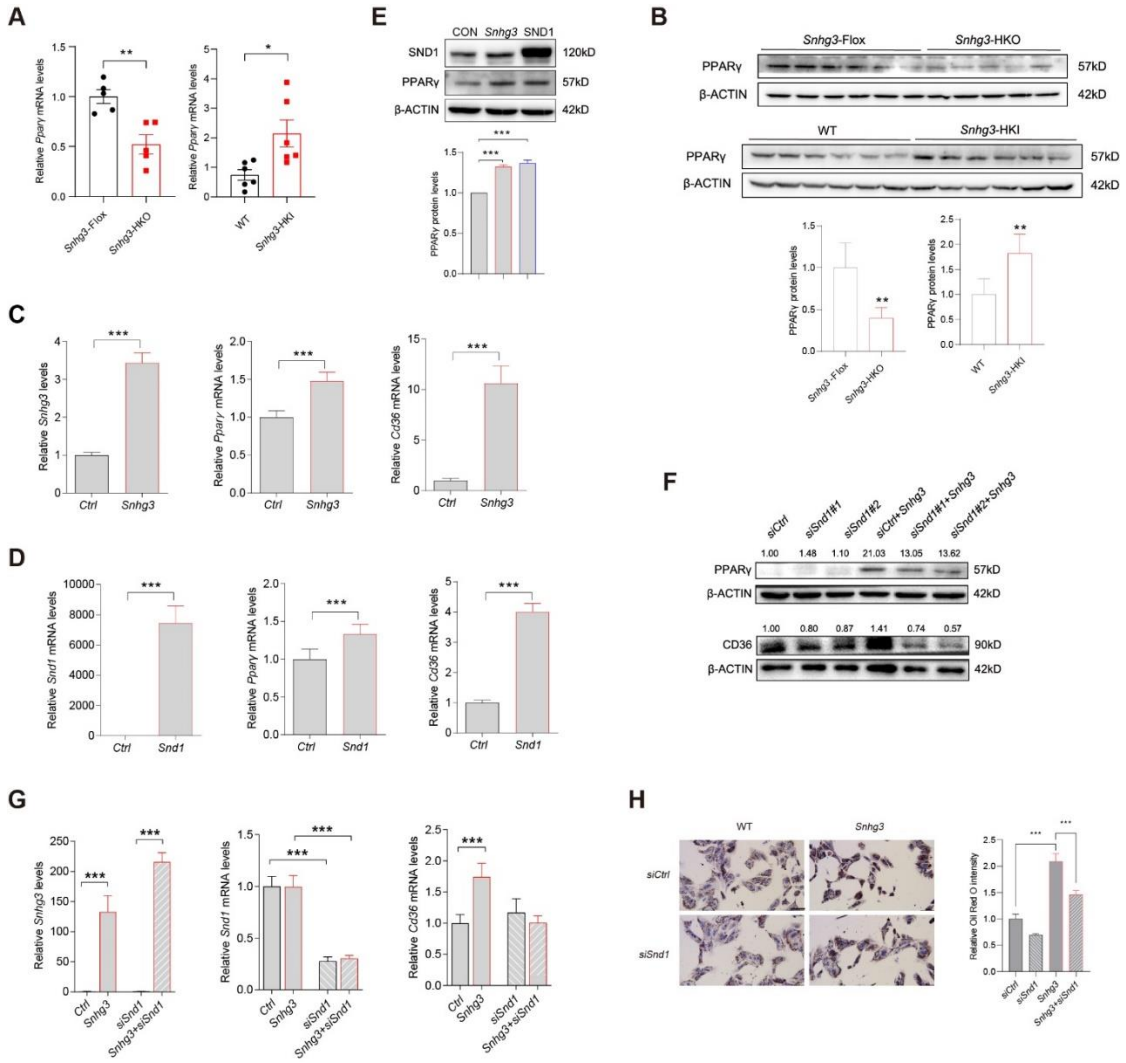

Figure 7. SND1 mediates *Snhg3*-induced PPARγ expression increase. (**A** and **B**) The mRNA (**A**) and protein (**B**, up, western blotting; down, quantitative result) expression level of PPARγ were measured *in vivo*. (**C** and **D**) Overexpression of *Snhg3* (**C**) and SND1 (**D**) promoted the mRNA expression of *Pparγ* and *Cd36* in primary hepatocytes. (E) Overexpression of *Snhg3* and SND1 increased the protein expression of PPARγ in Hepa1-6 cells (up, western blotting; down, quantitative result). (**F** - **H**) Disruption SND1 expression alleviated *Snhg3*-induced increase in the protein (**F**) and mRNA (**G**) levels of PPARγ and CD36, and lipid accumulation (**H**, left, oil red O staining; right, quantitative result) in primary hepatocytes with PA treatment. Data are

represented as mean ± SEM. *p < 0.05, **p < 0.01 and ***p < 0.001 by one-way ANOVA (**G** and **H**) or by Student's t test (the others).

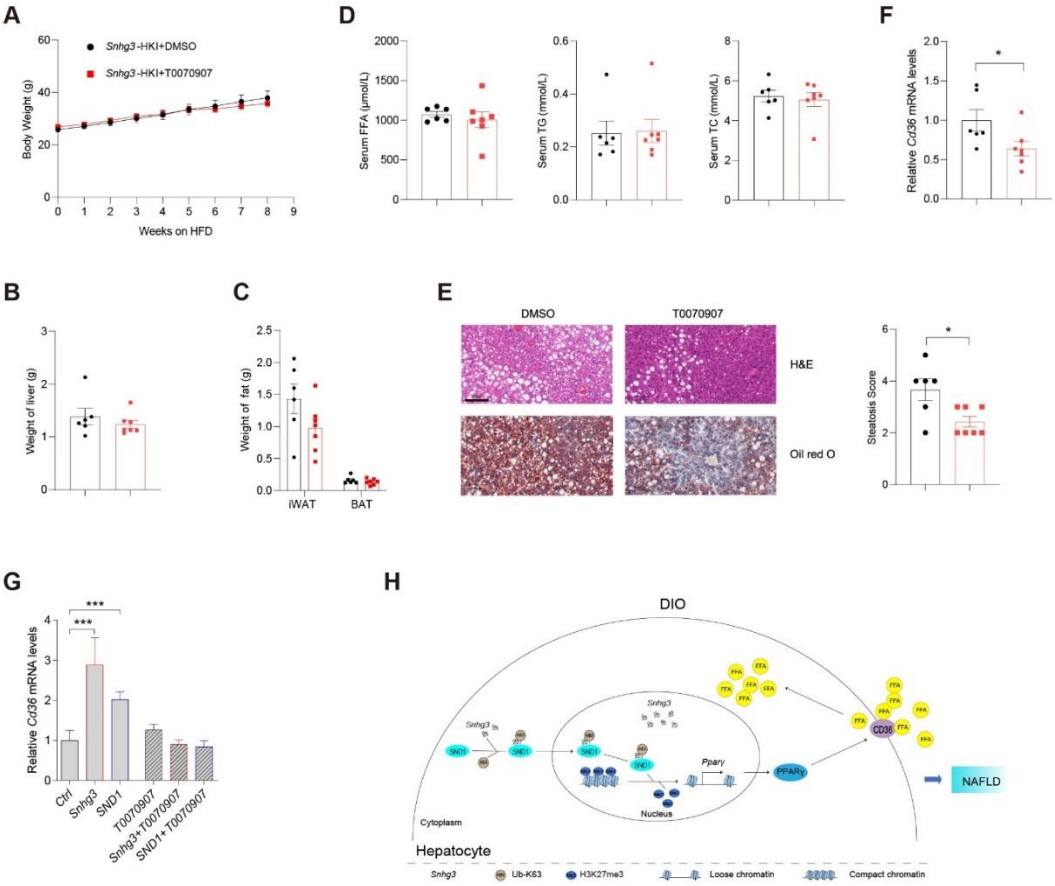

Figure 8. PPARγ mediates *Snhg3*-induced hepatic steatosis. (**A - C**) Body weights (**A**), liver weight (**B**) and adipose tissue weight (**C**) of DIO *Snhg3*-HKI mice without (n = 6) or with (n = 7) T0070907 treatment for 8 weeks. (**D**) Serum FFAs, TG and TG concentrations of mice as indicated in (**A**). (**E**) Hepatic H&E and oil red O staining (left) and NASH score (right) of mice as indicated in *A*. Scare bars, 100 μm. (**F**) T0070907 decreased hepatic *Cd36* expression in DIO *Snhg3*-HKI mice. (**G**) T0070907 disrupted *Snhg3*- and SND1-induced *Cd36* increase in Hepa1-6 cells. (**H**) Model of how *Snhg3* and SND1 interacting and influencing chromatin remodeling via H3K27me3, and promoting PPARγ expression thereby resulting in hepatic steatosis. Data are represented as mean ± SEM. *p < 0.05 and ***p < 0.001 by two-way ANOVA (**A**) or by Student's t test for the others.